A&A, 707, A3 (2026)
https://doi.org/10.1051/0004-6361/202558337

Astronomy & Astrophysics

Magnetic field detections in massive systems at different stages of interaction

S. Hubrig[1,⋆], M. Abdul-Masih[2,3], S. P. Järvinen[1], A. Cikota[4], M. Schöller[5], I. Ilyin[1], and A. Escorza[2,3]

[1] Leibniz-Institut für Astrophysik Potsdam (AIP), An der Sternwarte 16, 14482 Potsdam, Germany
[2] Instituto de Astrofisica de Canarias, C. Via Lactea, s/n, 38205 La Laguna, Santa Cruz de Tenerife, Spain
[3] Universidad de La Laguna, Departamento de Astrofisica, Av. Astrofisico Francisco Sanchez s/n, 38206 La Laguna, Tenerife, Spain
[4] Gemini Observatory/NSF's NOIRLab, Casilla 603, La Serena, Chile
[5] European Southern Observatory, Karl-Schwarzschild-Str. 2, 85748 Garching, Germany

Received 1 December 2025 / Accepted 3 January 2026

ABSTRACT

Context. Despite the importance of magnetic fields in massive stars, their origin is widely debated and still not well understood.
Aims. With the mounting evidence for the importance of studying magnetic fields in interacting massive binary and multiple systems, it appears necessary to investigate the presence of magnetic fields in semi-detached systems with ongoing mass transfer, and in contact systems where mass is actively being exchanged.
Methods. We present an analysis of 53 high-resolution HARPSpol spectropolarimetric observations of a sample of 14 massive binary and multiple systems using the least-squares deconvolution technique. The majority of the studied systems are classified as semi-detached or contact binaries.
Results. Definite detections of the presence of a magnetic field are achieved in all studied systems apart from the rather faint system SV Cen, for which only a marginal detection was obtained. The fact that the presence of magnetic fields is detected in all but one of the studied systems strongly suggests that interaction between the system components plays a definite role in the generation of magnetic fields in massive stars. The measured mean longitudinal magnetic field strength for all targets is of the order of a few hundred Gauss to a few kiloGauss. The strongest longitudinal magnetic fields of 4–5 kG are discovered in the massive O-type triple system MY Ser in both components of the contact binary. kiloGauss-order magnetic fields are also detected in two other systems, V1294 Sco and V606 Cen. It is possible that there is an implication of some system characteristics, such as multiplicity, the mass ratio between the components, and a large fillout factor, on the measured magnetic field strength. Our results for the magnetic field measurements in interacting binaries present the first assessment of the occurrence rate of magnetic fields in a representative sample of such systems.

Key words. techniques: polarimetric – binaries: eclipsing – binaries: spectroscopic – stars: magnetic field – stars: massive – stars: variables: general

1. Introduction

The important role of massive stars in the evolution of our Universe is widely recognised, but the origin of their magnetism and its impact on the stellar evolution and the ultimate fate of massive stars as supernovae and compact objects is still a matter of debate. The most popular scenario for the origin of the magnetic field involves a merging event, mass transfer, or a common envelope (CE) evolution. Mass transfer or stellar merging rejuvenate the mass gaining star (e.g. Tout et al. 2008; Ferrario et al. 2009; Schneider et al. 2016), while the induced differential rotation is thought to be the key ingredient to generate a magnetic field (e.g. Wickramasinghe et al. 2014). According to magnetohydrodynamical simulations of the merger of a binary by Schneider et al. (2019), shear between the accretion stream and the stellar surface forms a modest magnetic field, which is then bolstered considerably when the stellar cores merge. In the context of this scenario, massive O stars are of special interest for studies of their magnetism because more than 90% of them are born and live in binary or multiple systems (Offner et al. 2023) and up to 70% experience binary interaction during their life (e.g. Sana et al. 2012).

⋆ Corresponding author: shubrig@aip.de

Observational magnetic studies carried out in recent years have revealed that systems in different evolutionary states and different interaction phases indeed offer a way to disentangle different theoretically predicted magnetic field generation channels and, consequently, to understand the magnetic field origin. To test the importance of interaction processes for the generation of magnetic fields in massive stars, Hubrig et al. (2023) performed an analysis of 61 high-resolution spectropolarimetric observations of 36 systems with O-type primaries. The studied sample included multiple systems with components at different evolutionary stages with wide and tight orbits and different types of interaction. The authors reported that out of the 36 systems, 22 exhibited in their LSD Stokes V profiles definitely detected Zeeman features, 11 systems showed marginal evidence for the detection of a Zeeman feature, and 3 systems did not show the presence of a magnetic field.

From a theoretical point of view, the role of magnetic fields in close binary evolution is not yet clear. Usually, magnetic fields can be treated within magneto-hydrodynamical (MHD) simulations. However, according to Campbell (2018), the implementation of MHD in binary stars is very challenging because the presence of magnetic fields makes the range of physical phenomena extremely rich and complex. In addition to hydrodynamic

flow instabilities, MHD instabilities are important. The role of magnetic fields in the post-dynamical inspiral phase of CE evolution was recently discussed by Gagnier & Pejcha (2023), who suggested that an initially weak magnetic field may undergo amplification by interacting with spiral density waves and turbulence generated in the stellar envelope by the inspiraling companion. Also, jet-like outflows appear in the MHD simulations carried out by Ondratschek et al. (2022) and García-Segura et al. (2021). Given the very challenging numerical implementation of MHD, only observations of magnetic fields in binary and multiple systems at different stages of their interaction can give the crucial information necessary to test theoretical predictions on the magnetic field origin.

With the mounting evidence for the importance of studying magnetic fields in interacting massive binary and multiple systems, it appears necessary to investigate the presence and role of magnetic fields in semi-detached systems with ongoing mass transfer, and in systems in the contact phase directly preceding a merger event. Binary interactions can fundamentally alter the evolutionary path of a system, affecting the main sequence lifetime, the interior structures of the components, and the positions on the Hertzsprung Russell diagram (e.g. Marchant & Bodensteiner 2024). When the primary star in massive binaries fills its Roche lobe, mass transfer is initiated and the system enters a semi-detached configuration. In Roche lobe overflow (RLOF) interactions, three different cases are usually considered: case A, if the RLOF episode occurs when the mass donor is on the core hydrogen-burning main sequence; case B, when the star is in the hydrogen shell burning phase; and case C, when the star is in the helium shell burning phase (e.g. Kippenhahn & Weigert 1967; Vanbeveren et al. 1998). During the semi-detached phase, as mass is transferred from one component to the other, the mass receiver can expand and fill its Roche lobe as well, leading to a contact phase. The contact phase represents one of the most extreme forms of binary interactions throughout all branches of massive binary evolution. While in a contact configuration, the components share a common surface through which mass and energy are exchanged and experience a variety of interaction processes including but not limited to tidal locking, mutual illumination, internal mixing, and angular momentum exchange (Wellstein et al. 2001; de Mink et al. 2007). Henneco et al. (2024) identified five mechanisms that lead to contact and mergers: runaway mass transfer, mass loss through the outer Lagrange point L2, expansion of the accretor, orbital decay because of tides, and non-conservative mass transfer. The authors concluded that at least 40% of mass-transferring binaries with initial primary-star masses of 5–20 $M_{\odot}$ evolve into a contact phase; >12% and >19% likely merge and evolve into a CE phase, respectively.

To address questions on the magnetic field origin in massive stars, we recently obtained high-resolution ($R \approx 110\,000$) HARPSpol (High Accuracy Radial velocity Planet Searcher polarimeter; Snik et al. 2008) observations to explore the magnetic field incidence in a sample of close, semi-detached, and contact binaries. For a number of targets in our sample, the fillout factors, f, are known from the physical properties of the components, including their radii, the radii of the inner and outer Roche lobes, the surface potentials of the components, and the surface potentials of the inner and outer Roche lobes. According to Mochnacki & Doughty (1972), fillout factors describe the degree to which the equipotential surface corresponding to the photosphere fills out the Lagrangian zero-velocity surfaces. For detached components, which have photospheres lying inside their inner Lagrangian surfaces, the fillout factor is $0 < f \leq 1$, whereas for contact configurations the photosphere lies between the first and second Lagrangian surfaces corresponding to $1 \leq f \leq 2$. Very few such systems have previously been analysed using spectropolarimetric observations. The presence of rather strong longitudinal magnetic fields has been reported for the well-known contact binaries MY Ser (=HD 167971) and LY Aur (=HD 35921) by Hubrig et al. (2023), who used ESPaDOnS archival observations. More recently, the presence of a magnetic field was detected in the primary of the suspected contact ON3 If*+O5.5 V((f)) binary system NGC 346 SSN 7 ($P_{\rm orb}$ = 3.07 d) located in the Small Magellanic Cloud using low-resolution observations with the ESO/VLT FOcal Reducer low dispersion Spectrograph (FORS2; Appenzeller et al. 1998) in spectropolarimetric mode (Hubrig et al. 2024).

Notably, observational surveys of the presence of magnetic fields in contact systems are severely hampered by the frequent occurrence of these systems in higher order multiple systems. According to Abdul-Masih (2025), of the confirmed contact systems, almost 70% have at least one confirmed companion and about 25% have more than one additional companion. The majority of these detections come through eclipse timing variations (ETVs) due to the light travel time effect, spectroscopic studies, and interferometry. Abdul-Masih (2025) suggests that due to the compactness of the inner orbits in such systems, their multiplicity properties may be fundamentally different from those of other O-type systems. Pablo et al. (2018) mentioned several other obstacles in studies of contact systems. Spectral lines of the components usually have significant overlap at most binary phases, preventing accurate radial velocity measurements. Further, in such systems surfaces are illuminated by two separate energy sources, making the determination of the temperature distribution difficult.

In this work, we present our analysis of 53 high-resolution HARPSpol spectropolarimetric observations acquired over the last two years for fourteen massive binary and multiple systems with components at different evolutionary stages undergoing different types of interaction. In Sect. 2 of this article, we detail our spectropolarimetric observations and describe the methodology of the data analysis. The results of the magnetic field measurements for each target are presented in Sect. 3. In Sect. 4, we discuss the implication of the reported magnetic field detections for future studies of massive stars.

2. Observations and analysis

Our spectropolarimetric observations were carried out on January 2 and 4 and on June 17 to 20 in 2024 and on April 12 to 16 2025 using HARPSpol attached to ESO's 3.6 m telescope on La Silla. HARPSpol has a resolving power of about 110 000 and a wavelength coverage from 3780 to 6910 Å, with a small gap between 5259 and 5337 Å. The normalisation of the spectra to the continuum level was described in detail by Hubrig et al. (2013). One additional spectropolarimetric observation of 29 CMa with ESPaDOnS (the Echelle SpectroPolarimetric Device for Observations of Stars) acquired on March 3 2013 was retrieved from the CFHT (the Canada-France-Hawaii Telescope) science archive. ESPaDOnS covers the wavelength range from 3750 to 10 500 Å and the spectral resolution of the ESPaDOnS observations is about 65 000.

With HARPSpol and ESPaDOnS, we have access to measurements of the mean longitudinal magnetic field $\langle B_z \rangle$, which is the line-of-sight component of the magnetic field, weighted with the line intensity and averaged over the visible hemisphere. The longitudinal magnetic field is strongly dependent on the viewing

Table 1. Sample of the investigated multiple systems.

Target	m_V	Spectral classification	Ref.	Multiplicity	Ref.	Notes	Ref.
γ Equ	4.7	A9 Vp SrEu	(1)	Single		Standard	
29 CMa	5.0	O9 Iabf+O9.7 Ib	(2)	SB2?	(2)	Contact?	(20)
V402 Pup	9.2	O6 V+O6 V, O9.5 V+O9.5 V	(3)	Quadruple	(3)	Contact	(3)
TU Mus	9.3	O7 V+O8 V	(4)	Quadruple?	(16)	Contact	(16)
SV Cen	9.7	B6.5III+B2V	(5)	SB2	(5)	Semi-detached?	(21)
V606 Cen	9.7	B0.5 V+B3 V	(6)	Triple	(17)	Contact	(17)
V889 Cen	11.7	O4f$^+$+O6-7:(f):	(7)	SB2	(7)	Contact	(7)
V918 Sco	5.5	O7.5 I(f)+ON9.7	(8)	SB2	(18)	BSG, CWB, post-RLOF	(18)
HR 6187	5.7	O3-3.5 V+O5.5-6 V+O6.5-7 V	(9)	Triple	(9)	CWB, merger?	(9)
μ^{01} Sco	3.0	B1.5 V+B8-B3	(10)	SB2	(10)	Semi-detached	(10)
V1294 Sco	7.6	O9.5IV(n)+B0V	(11)	SB2	(11)	Detached?	(22)
V701 Sco	9.0	B1-1.5 V+ B1-1.5 V	(12)	Triple?	(12)	Contact	(12)
MY Ser	7.5	O7.5III+O9.5III+O9.5I	(13)	SB3	(19)	PACWB, contact	(23)
V356 Sgr	7.0	A2I+B3V	(14)	SB2	(14)	Contact?	(14)
V337 Aql	8.9	B0+B3	(15)	SB2	(15)	Semi-detached	(15)

Notes. The first column gives the target name and the second column the visual magnitude. In Columns 3 and 4, we present for each target the spectral classification and the corresponding reference. The multiplicity indicator and the corresponding reference are listed in Columns 5 and 6. Here, the entries SB2/3 correspond to spectroscopic binaries with double and triple line systems, and '?' to a multiplicity classification uncertainty. Columns 7 and 8 list notes concerning the interaction status of the system members and the corresponding reference. BSG stands for blue supergiants, CWB for colliding wind binaries, and PACWB for particle-accelerating colliding-wind binaries exhibiting synchrotron radio emission. References: (1) Bychkov et al. (2016); (2) Bagnuolo et al. (1994); (3) Lorenzo et al. (2017); (4) Penny et al. (2008); (5) Drechsel (1994); (6) Lorenz et al. (1999); (7) Raucq et al. (2017); (8) Sota et al. (2014); (9) Mahy et al. (2018); (10) van Antwerpen & Moon (2010); (11) Maíz-Apellániz et al. (2004); (12) Qian et al. (2006); (13) De Becker (2018); (14) van Rensbergen et al. (2011); (15) Tüysüz et al. (2014); (16) Qian et al. (2007); (17) Li et al. (2022); (18) Thaller (1998); (19) Ibanoglu et al. (2013); (20) Pablo et al. (2018); (21) Rucinski et al. (1992); (22) Rosu et al. (2022); (23) De Becker & Raucq (2013).

angle between the field orientation and the observer and is modulated as the star rotates. The assessment of the longitudinal magnetic field measurements is presented in our previous papers (e.g. Hubrig et al. 2018; Järvinen et al. 2020). Similar to our previous studies, to increase the signal-to-noise ratio (S/N) by a multi-line approach, we employed the least-squares deconvolution (LSD) technique. The details of this technique, as well as how the LSD Stokes I, Stokes V, and diagnostic null spectra are calculated, were presented by Donati et al. (1997).

Several complications existing in the analysis of the presence of magnetic fields in multiple systems have recently been discussed in the work by Hubrig et al. (2023). The amplitudes of the Zeeman features (the features appearing in the Stokes V spectra of magnetic stars) are much lower in multiple systems in comparison with their size in single stars. These features also appear blended in composite spectra and can show severe shape distortions. Also the shapes of blended spectral lines in the Stokes I spectra look different depending on the visibility of each system component at different orbital phases. The number of spectral lines suitable for the LSD technique analysis for massive stars is in addition much lower in comparison to less massive stars. Furthermore, special care has to be taken to populate the LSD line masks for each system because the composite spectra of multiple systems usually show very different spectral signatures corresponding to the different spectral classification of the individual components.

Therefore, we searched in the Stokes V spectra of O and B-type systems for both Zeeman features with typical and atypical shapes. To evaluate whether the detected features are spurious or definite detections, we followed the generally adopted procedure to use the false alarm probability (FAP), based on reduced χ^2 test statistics (Donati et al. 1992): the presence of the Zeeman feature is considered as a definite detection (DD) if FAP $\leq 10^{-5}$, as a marginal detection (MD) if $10^{-5} <$ FAP $\leq 10^{-3}$, and as a non-detection (ND) if FAP $> 10^{-3}$. The list of targets, their visual magnitudes, spectral classifications, multiplicity information, and interaction status, together with the related literature sources, are presented in Table 1.

3. Results of our LSD analysis for individual targets

In the following, we give a brief description of the targets in our sample and discuss the results of the magnetic field measurements for each target individually. These results are also summarised in Table A.1.

γ Equ (=HD 201601). The typical strongly magnetic Ap star γ Equ was used as a standard star during our observations in 2024. Because of its high brightness and the extremely long rotation period $P_{\rm rot} > 97$ yr (Bychkov et al. 2016), this star is frequently used as a magnetic standard to test the functionality of spectropolarimetric devices at different telescopes. We used in our LSD analysis HARPSpol observations of γ Equ acquired on July 24 2011, on June 18 2024, and on July 5 2025, applying a mask containing lines belonging to iron and rare earth elements. In Fig. 1, we demonstrate that the strength of the longitudinal magnetic field is gradually decreasing from −1534 G in 2011 to −964 G in 2025. The intensities of the LSD Stokes I profiles presented in this figure on the right side are also decreasing over the same time interval.

29 CMa (=HD 57060). Using archival IUE spectra, Bagnuolo et al. (1994) reported for this eclipsing binary a spectral classification O7.5-8 Iabf for the primary and O9.7 Ib

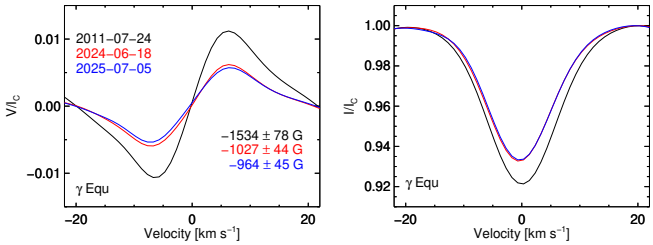

Fig. 1. LSD Stokes profiles of the standard star γ Equ. *Left* LSD Stokes V profiles for the HARPSpol observations of γ Equ from 2011 to 2025. *Right* Intensities of the LSD Stokes I profiles of γ Equ at different observational epochs.

for the secondary and respective masses 19 $M_\odot$ and 16 $M_\odot$, i.e. a mass ratio of $q = M_2/M_1 = 0.84$ (Sen et al. 2022). The system is expected to be in a contact configuration and the light curve analysis of photometric observations obtained during the Hipparcos mission yielded an orbital period of 4.39336 d (Antokhina et al. 2011). However, since spectroscopic material was not available at that time, it was not possible to determine the mass ratio from the light curve solution alone. Using BRITE and SMEI photometry in conjunction with concurrent spectroscopy for the analysis of this system, Pablo et al. (2018) confirmed previously reported asymmetries in the light curve (e.g. Leung & Schneider 1978), which are difficult to model effectively. The authors also found the presence of an unexplained frequency at twice that of the orbit. So far, no convincing radial velocity curve of the secondary has been presented in the literature and attempts to fit both the light curve and the radial velocity curve simultaneously have resulted in unreliable combined fits, bringing its orbital configuration into question. Burssens et al. (2020) reported 29 CMa as an SB1 from IACOB/OWN spectroscopy, in addition to wind variability in emission. Further, they detected in the one-sector TESS data large amplitude eclipses with a period of 4.40(6) d.

Five HARPSpol observations were acquired in January and June 2024 and one observation in April 2025. An additional ESPaDOnS observation of this system from 2013 was retrieved from the CFHT (the Canada–France–Hawaii Telescope) scientific archive. Clear Zeeman signatures in the LSD Stokes V profile calculated using various masks including He I/II, C IV, N III, O II/III, and Si III/IV lines are well visible in all observations and correspond to the more massive component. As is demonstrated in Fig. B.1 and in Table A.1, definite detections are achieved in the ESPaDOnS observation, and the HARPSpol observations on June 17 and 19 2024 and April 15 2025. The longitudinal magnetic field is variable and shows a change of polarity, with the strongest positive field $\langle B_z \rangle = 298 \pm 59$ G (FAP $< 10^{-10}$) measured on June 19 2024 and the strongest negative field $\langle B_z \rangle = -159 \pm 113$ G (FAP $< 10^{-10}$) measured on June 17 2024. The presence of a magnetic field in 29 CMa was also confirmed in the recent low-resolution observation carried out on November 10 2024 using the ESO multi-mode instrument FORS2. The longitudinal magnetic field $\langle B_z \rangle = -183 \pm 59$ G was detected at a significance of 3.1σ (*in preparation*).

V402 Pup (=HD 64315). Lorenzo et al. (2017) reported that V402 Pup is a multiple system consisting of two binary systems, one of which, V402 Pup BaBb, is an eclipsing binary. The two binary systems are separated by about 0.09″. The components of the eclipsing binary V402 Pup BaBb with an orbital period of 1.019 d have spectral types O9.5 V+O9.5 V and almost identical masses of 14.6 $M_\odot$. Both components in the eclipsing system are overfilling their respective Roche lobes, sharing a common surface. In a recent overview of massive contact binary observations, Abdul-Masih (2025) reported a fillout factor of $f = 1.31$. The non-eclipsing binary V402 Pup AaAb is a detached system with an orbital period of 2.710 d and is composed of two stars with spectral types around O6 V. Lorenzo et al. (2017) suggest a minimum mass of 10.8 $M_\odot$ for the primary and 10.2 $M_\odot$ for the secondary, and a mass ratio $q = 0.94$.

The presence of four components in the system V402 Pup complicates the search for the presence of a magnetic field. Lorenzo et al. (2017) reported that the lines corresponding to V402 Pup BaBb are mostly hidden within the complex and broad profiles generated by the more luminous components of the system V402 Pup AaAb, but each of the four components contributes to every spectrum in the He I, He II, and Balmer lines. The system was observed with HARPSpol twice in April 2025. As is presented in Fig. B.2 and Table A.1, using a mask with the He I/II lines for the first observation on April 15, 2025, we detect in the LSD Stokes V spectrum a narrow Zeeman signature with FAP $= 9 \times 10^{-5}$ corresponding to a marginal detection. For the second observation on April 16 2025 showing all components overlapped, we detect a rather broad Zeeman signature with FAP $= 2 \times 10^{-6}$ using a mask containing He I/II and O III lines. For this observation we measure a definite longitudinal magnetic field $\langle B_z \rangle = 353 \pm 67$ G. Due to the complexity of this multiple system, it is not clear which component(s) in which system possess a magnetic field.

TU Mus (=HD 100213). According to Penny et al. (2008), the spectral types of the components in the eclipsing binary with an orbital period of 1.387 d are O7 V+O8 V with corresponding masses of 16.7 $M_\odot$ and 10.4 $M_\odot$, respectively. Their analysis indicated that both stars are currently experiencing RLOF. In a recent overview of massive contact binary observations, Abdul-Masih (2025) reported a fillout factor of $f = 1.12$. With a mass ratio of 0.623, TU Mus is one of the most unequal mass contact systems (Abdul-Masih et al. 2022). The periodic changes in the orbital period of the system detected by Qian et al. (2007) suggest that it contains a third much fainter component with the lowest mass in the system of 1.55 $M_\odot$. This study also revealed the presence of a distant fourth visual companion at a separation of 16″ southeast of TU Mus. The existence of additional components in TU Mus probably plays an important role for their formation and evolution by removing angular momentum from the central system (Qian et al. 2007).

TU Mus was observed three times, twice in June 2024 and once in April 2025. As is presented in Fig. B.3 and Table A.1, using a line list containing He I/II lines, we detect a definite magnetic field $\langle B_z \rangle = 482 \pm 198$ G with FAP $= 10^{-5}$ in the first observation on June 18 2024. In this orbital phase the binary components appear overlapped. The components are well separated during the second observation one day later, but the Zeeman signature detected using He I/II lines is marginal with 7×10^{-4}. The position of the definitely detected Zeeman signature on April 14 2025 with FAP $= 2 \times 10^{-6}$ using a mask with He I/II and C IV lines probably indicates that the more massive component in the eclipsing binary possesses a magnetic field.

SV Cen (=HD 102552). This system consists of two components with spectral types B1.5 V and B6.5 III (Drechsel 1994), with masses of 8.56 $M_\odot$ and 6.05 $M_\odot$ ($q = 0.71$) (van Rensbergen et al. 2011), respectively. Both components in a tight 1.66 d orbit apparently undergo a very rapid orbital evolution. The configuration of this system has been widely debated in the literature.

Some studies claim that it is a contact system (e.g. Rucinski et al. 1992; Drechsel 1994), while others claim that it is semi-detached (e.g. De Greve & Linnell 1994; Deschamps et al. 2013; Davis et al. 2014). While contact systems evolve on a nuclear timescale, the recent analysis of SV Cen by Vrancken et al. (2024) suggests that SV Cen is evolving on a thermal timescale. This indicates that the configuration is more likely semi-detached instead of contact. According to the work of these authors, most of the studied contact systems have a period stability of at least ∼1 Myr up to 20 Myr, while for SV Cen it is about 0.05 Myr.

One spectropolarimetric observation for this relatively faint target was carried out on June 19 2024. As is presented in Fig. B.4 and Table A.1, the Zeeman signature is only marginally detected (FAP = 10^{-3}) using a mask with He I and Si III lines. The position of this signature relative to the Stokes I spectrum showing separated components suggests an association with the less massive component.

V606 Cen (=HD 115937). The components of the rather faint eclipsing contact binary V606 Cen with an orbital period of 1.495 d have spectral types B0-B0.5 V for the primary with a mass of 14.7 $M_\odot$ and B2-B3 V for the secondary component with a mass of 8.0 $M_\odot$ (Lorenz et al. 1999). By analysing the continuous light curve obtained by TESS, Li et al. (2022) found that it is a marginal contact binary with a very low fillout factor of about 2%. Both the marginal contact configuration and the continuous period decrease suggest that V606 Cen is a newly formed contact binary via case A mass transfer. Their results also indicated that V606 Cen is a member in a hierarchical triple system: the cyclic change in the O–C diagram was explained by the light-travel time effect via the presence of a third body, with the tertiary having the lowest mass in the system of 4.51 $M_\odot$. The tertiary is orbiting the central eclipsing binary with q = 0.5484 in an excentric orbit with e = 0.33.

This system was observed twice each in June 2024 and April 2025. As is presented in Fig. B.5 and Table A.1, while only a marginal detection of a Zeeman signature (FAP = 4×10^{-4}) was achieved for the first observation on June 18 2024, showing overlapped binary components, we achieved a definite detection $\langle B_z \rangle = -419 \pm 168$ G with FAP = 2×10^{-6} on June 19 2024 using a mask with He I/II, and Si III lines. A second definite detection, $\langle B_z \rangle = 1327 \pm 128$ G with FAP < 10^{-10} was obtained on April 14 2025 using a mask containing He I/II, Al III, and Si III lines. The positions of the Zeeman signatures relative to the composite Stokes I spectrum indicate that the magnetic field is detected in the more massive component. No detection was achieved on April 14 2025 with a mask containing He I/II, Al III, and Si III lines.

V889 Cen (=LSS 3074). With m_V = 11.7, this system is the faintest in our sample. Thus the S/N values for the obtained spectra are very low, in the range from 24 to 49. The orbital parameters of this short-period spectroscopic binary with masses of 14.8 $M_\odot$ for the primary and 17.2 $M_\odot$ for the secondary (q = 0.86) and spectral types O4f$^+$ and O6-7:(f):, respectively, were reported by Raucq et al. (2017). The authors assumed a circular orbit and an orbital period of 2.1852 days. An analysis of the light curve indicated that V889 Cen is a candidate for a contact binary with f = 1.05 and has lost a significant portion of its mass to its surroundings. According to Abdul-Masih et al. (2022), the photometric analysis strongly favours a contact configuration over a semi-detached configuration. Raucq et al. (2017) detected a strong overabundance in nitrogen and a strong carbon and oxygen depletion in the atmospheres of both primary and secondary, and a strong helium enrichment of the primary star.

V889 Cen was observed two times in June 2024 and three times in April 2025. As is presented in Fig. B.6 and Table A.1, using a line mask containing He I/II lines we achieved a definite detection of a Zeeman signature with FAP < 10^{-9} on June 20 2024 and a marginal detection using a mask containing He I/II and C IV lines with FAP = 6×10^{-4} one day later. In the observations carried out in 2025, using a mask with He I/II and C IV lines, we achieved definite detections of a Zeeman signature with FAP = 6×10^{-7} and FAP < 10^{-10} on April 14 and 16, 2025, respectively. No Zeeman signature was detected on April 15, 2025. The positions of the detected Zeeman signatures relative to the composite Stokes I spectrum indicate that the magnetic field is present in the less massive component. However, due to the fact that in our low-S/N spectra the secondary component is not well separated, we are not able to measure the longitudinal magnetic field corresponding to the detected Zeeman signatures.

V918 Sco (=HD 149404). According to Rauw et al. (2001), the ON9.7 I secondary in this system is on a circular orbit with a period of 9.81 d around the O7.5 I(f) primary and seems to be the most evolved component. Raucq et al. (2016) reported 50.5 $M_\odot$ for the primary and 31.9 $M_\odot$ for the secondary. and that the current evolutionary status of V918 Sco could best be explained if the system has undergone a RLOF episode in the past. The authors detected a large overabundance in nitrogen and a carbon and oxygen depletion in the secondary star and also found a slight nitrogen enhancement in the primary's spectrum. Furthermore, they inferred an asynchronous rotation of the two stars of the system. It is also possible that both components emit powerful, radiatively driven stellar winds. Thaller (1998) suggested that the double-peaked structure of the Hα emission observed in this system is due to colliding wind interaction. Also Rauw et al. (2001) favoured a model where the Hα emissions arise in the arms of a colliding wind shock region.

The presence of a magnetic field in V918 Sco was recently studied by Hubrig et al. (2023), who used for the LSD analysis one HARPSpol observation obtained in 2016 and one ESPaDOnS observation acquired in 2014. For both observations the authors achieved marginal detections with FAP = 5×10^{-4} and FAP = 7×10^{-4}, respectively. As is shown in Fig. B.7 and Table A.1, this system was observed four more times. We achieved definite detections in both observations obtained in June 2024 and in the second observation acquired in April 2025. The longitudinal magnetic field is rather weak with $\langle B_z \rangle$ = 45 ± 31 G and FAP = 6×10^{-6} measured on June 20 2024 using a mask containing He I/II, C IV, N III, and Si III lines. The first observation in April 2025 showed a marginal detection $\langle B_z \rangle$ = −11 ± 6 G with FAP = 4×10^{-4} using a mask with He I/II, C IV, N III, and O III lines.

HR 6187 (=HD 150136). This triple hierarchical system is formed by an inner binary with an O3 V((f*))–O3.5 V((f+)) primary and an O5.5–6 V((f)) secondary orbiting around each other with a period of 2.67455 d, and an O6.5–7 V((f)) physically bound tertiary component located on a much longer orbit of about 8.2 yr (Mahy et al. 2018). By combining spectroscopy, interferometry, and photometry for this triple system, Mahy et al. (2018) showed that the masses estimated through their analysis (42.8 $M_\odot$, 29.5 $M_\odot$, and 15.5 $M_\odot$) are much smaller than those expected from evolutionary models (55.4 $M_\odot$, 30.6 $M_\odot$, and 22.4 $M_\odot$). This indicates that a merge or mass transfer took place in this system.

Only one HARPS pol observation has been acquired for this triple system. As is demonstrated in Fig. B.8 and Table A.1, we achieved a definite detection $\langle B_z \rangle = 369 \pm 58$ G with FAP = 6×10^{-6} using a mask with He I/II, C IV, and N III. Since in the LSD Stokes I spectrum all components appear overlapped, it is not obvious which component hosts the magnetic field.

μ^{01} Sco (=HR 6247). The components of this bright eclipsing system ($m_V = 2.98$) with an orbital period of 1.446 d have spectral types B1.5 V and B8-B3 and masses 8.49 $M_\odot$ and 5.33 $M_\odot$, respectively (van Antwerpen & Moon 2010). Using photometric and spectroscopic data, Budding et al. (2015) suggested for the masses of the components 8.3 $M_\odot$ and 4.6 $M_\odot$ ($q = 0.55$). The authors confirmed the results of previous studies, which reported that the secondary star is larger than the primary, and certainly larger than a normal main-sequence relationship would imply for the given primary radius and the secondary's much lower mass. Accordingly, the system must be in a state of interactive evolution. Earlier studies suggested appreciable mass-loss from the system in the relatively recent past (e.g. Stickland et al. 1996). This conclusion was based on the assumption of Algol-like conditions. However, the work of Budding et al. (2015) showed that the relatively high masses of the components, the high primary surface temperature, and the proximity of the components do not indicate an Algol-like nature of this binary. Using Gaia data, Gratton et al. (2023) reported that the system has a distant companion with a mass of 0.48 $M_\odot$ at a separation of 44″.

Our observations were carried out on four different epochs in June 2024 and on seven different epochs in April 2025. As is presented in Fig. B.9 and Table A.1, out of the eleven observations, definite detections were achieved in five observations, marginal detections in four observations and non-detections in two observations. Given the spectral types of the components, we used line masks containing He I and Si II/III lines. For one observation on June 18, 2024 with a definite detection, we were able to estimate for the more massive component a mean longitudinal magnetic field $\langle B_z \rangle = 242 \pm 55$ G with FAP = 10^{-5}. A longitudinal magnetic field $\langle B_z \rangle = -187 \pm 29$ G for the same component was measured for one observation in June 19, 2024 with a marginal detection (FAP = 2×10^{-4}). A mask containing He I and Si III lines was used for both measurements.

V1294 Sco (=HD 152218A). According to Rosu et al. (2022), V1294 Sco is an eclipsing eccentric binary system with an orbital period of 5.6 d and components with masses of 20.6 $M_\odot$ and 15.5 $M_\odot$ ($q = 0.75$) and corresponding spectral types O9 IV for the primary and O9.7 V for the secondary (Sana et al. 2008). The rotation periods for the primary and the secondary are 2.69 and 2.56 d, respectively. The authors reported the lack of a secondary eclipse in photometric observations, which induces degeneracies between the primary and secondary Roche lobe filling factors and the inclination of the system. Due to the quite high eccentricity of the system of about 0.28 and the absence of an enhanced nitrogen abundance, Rauw et al. (2016) suggested that the components in V1294 Sco did not interact in the past.

This system was already observed with HARPSpol in the past twice and reported as magnetic by Hubrig et al. (2023). While the first observation in 2013 with both components blended with each other yielded a non-detection, the second HARPSpol observation from 2016 revealed a clear Zeeman feature with FAP < 10^{-10} corresponding to a longitudinal magnetic field $\langle B_z \rangle = -307 \pm 94$ G in the secondary less massive component. As is presented in Fig. B.10 and Table A.1, we confirm the magnetic nature of this system. We achieved in all newly obtained three HARPSpol observations definite detections and measure on April 15 2025 a rather strong mean longitudinal magnetic field in the secondary component, $\langle B_z \rangle = 1559 \pm 131$ G with FAP < 10^{-10}, using a line mask with He I/II, C IV, and Si III lines. The binary components in the two other observations appeared partly overlapped, preventing us from measuring the magnetic field.

V701 Sco (=HD 317844). This contact eclipsing binary with an orbital period of 0.761875 d is composed of two B1-1.5V type stars (Qian et al. 2006) with stellar masses of 9.78 $M_\odot$ and 9.74 $M_\odot$, respectively, and is still on the stage of a slow case A mass transfer (Yang et al. 2019). Eggen (1961) suggested that the two almost identical components of V701 Sco are zero-age-main-sequence stars in the young open galactic cluster NGC 6383. According to Qian et al. (2006), this contact binary has been formed by the fission of the third body by bringing angular momentum for the central system and creating a contact configuration of identical components. A fillout factor of $f = 1.55$ and the possible presence of an additional component was reported by Yang et al. (2019).

This system was observed once in June 2024 and three times in April 2025. As is presented in Fig. B.11 and Table A.1, we achieved definite detections of the Zeeman signatures for three observations. A longitudinal magnetic field $\langle B_z \rangle = 678 \pm 150$ G (FAP = 10^{-7}) was measured on June 19 2024. We detected a change of polarity for the marginal detection $\langle B_z \rangle = -876 \pm 105$ G (FAP = 4×10^{-4}), achieved on April 12, 2025. For all observations we used a mask containing He I and Si III lines. Taking into account the orbital period of 0.761875 d, we conclude that both B-type components are magnetic.

MY Ser (=HD 167971). According to Ibanoglu et al. (2013), this SB3 system is one of the rare massive O-type triple systems where the secondary and the tertiary components compose an eclipsing binary. The spectral types of the stars in the close binary are O7.5 III (component Aa) and O9.5 III (component Ab), and O9.5 I (component B) for the tertiary. The corresponding masses are 32.23 $M_\odot$ for the primary and 30.59 $M_\odot$ for the secondary ($q = 0.95$) in the close binary, and 29 $M_\odot$ for the tertiary. The brighter component Aa/Ab of this triple system is a contact eclipsing binary with an orbital period of 3.3216 d, just filling the entire outer contact surface with a fillout factor of 1.99. The outer pair AaAb/B has a period of about 21.2 yr. MY Ser was also classified as a particle-accelerating colliding-wind binary (PACWB) exhibiting synchrotron radio emission (De Becker & Raucq 2013). This system is also known to be one of the brightest synchrotron radio emitters.

The presence of a rather strong magnetic field was already reported by Hubrig et al. (2023), who used two ESPaDOnS archival observations from 2013 and 2017. A Zeeman signature with FAP < 10^{-10} in the first observation corresponding to $\langle B_z \rangle = 1324 \pm 582$ G was detected in the weakest red component B. Zeeman signatures for two components were detected in the second ESPaDOnS observation where a marginal detection with FAP = 9×10^{-4} corresponding to $\langle B_z \rangle = -977 \pm 437$ G was achieved for the blue component Aa and a definite detection with FAP = 6×10^{-6} corresponding to $\langle B_z \rangle = -57 \pm 33$ G was achieved for the central component B, showing the deepest intensity profile in the Stokes I spectrum. No detection was achieved for the third component.

Four new HARPSpol observations were acquired on three consecutive nights in June 2024 and on one night in April 2025. As is presented in Fig. B.12, similar to previous observations, all three components and corresponding Zeeman signatures are well visible in all LSD Stokes I and V spectra. Our result for the magnetic field measurement in the central component B in the first observation obtained on June 18 2024, $\langle B_z \rangle = -46 \pm 31$ G with FAP = 1×10^{-7} and using a line mask containing He I/II, C III, N III, O III, and Si IV lines, is in agreement with the result by Hubrig et al. (2023), suggesting that this component is weakly magnetic. The field measurement in the blueshifted weak component Ab using a mask containing He I, C III/IV, and O III lines for the second observation obtained on June 19 2024 revealed the presence of an extremely strong longitudinal field, $\langle B_z \rangle = 4008 \pm 402$ G with FAP = 2×10^{-8}. Taking into account the orbital period of MY Ser of 3.3216 d and the radial velocity variability presented in Figure 2 in the study of Ibanoglu et al. (2013), this strong field belongs to the more massive binary component Aa. Applying a mask with He I/II, C III, and O III lines, the detected redshifted Zeeman signature in the third observation on June 20, 2024 corresponds to the lower-mass component Ab in the eclipsing binary. We achieved for this observing epoch a definite detection with FAP < 10^{-10}, but are not able to estimate the field strength due to the weakness of this component. A definite magnetic field for the same component Ab, $\langle B_z \rangle = -4875 \pm 394$ G with FAP = 2×10^{-8}, was measured in the observation acquired on April 16 2025 using a mask with He I/II and C III lines. In this last observation, the lower-mass component Ab is shifted from the position of the central component B to the red, while the more massive component Aa is shifted to the blue. Using a mask with He I/II, N III, and O III lines, we achieved for the more massive component Aa a marginal detection (FAP = 4×10^{-5}) and measure a longitudinal field $\langle B_z \rangle = 8619 \pm 662$ G. In view of the previously reported detection of strong synchrotron radio emission in this system, it is quite possible that its generation is directly related to the presence of extremely strong magnetic fields in both binary components.

V356 Sgr (=HD 173787). According to Lomax et al. (2017), this system is considered as an eclipsing RLOF system and is morphologically similar to the β Lyr system. Both systems, V356 Sgr and β Lyr, are undergoing RLOF, which has caused discs to form around their gainers. However, in contrast to the β Lyr system, the accretion disc in the V356 Sgr system is optically thin. It was suggested that the 3 $M_\odot$ A2 supergiant secondary star has filled its Roche lobe and is currently transferring matter to the brighter, B3 V primary star with a mass of 11 $M_\odot$ (e.g. van Rensbergen et al. 2011). The orbital period of 8.9 d is reported in the work of van Hamme & Wilson (1990).

V356 Sgr was observed with HARPSpol on two nights in June 2024. As is shown in Fig. B.13 and Table A.1, we detected definite longitudinal magnetic fields in both observations. Using a line mask with He I, Si II/III, and Fe II lines we measured $\langle B_z \rangle = 856 \pm 240$ G with FAP = 1.5×10^{-7} for the B3 V component in the first observation obtained on June 18 2024. Using a mask with Mg II and Fe II lines, we obtained $\langle B_z \rangle = -718 \pm 245$ G with FAP = 7×10^{-6} for the A2 component in the second observation obtained on June 20 2024.

V337 Aql (=HD 177284). The simultaneous light and radial velocity curves solution by Tüysüz et al. (2014) indicated for this β Lyr type eclipsing binary system with an orbital period of 2.7339 d a mass of 17.44 $M_\odot$ for the primary and 7.83 $M_\odot$ for the secondary. The authors suggested that this B0+B3 system is a near-contact semi-detached binary, in which a primary star is inside its Roche lobe with a filling ratio of 92% and the secondary star fills its Roche lobe.

We obtained three HARPSpol observations, two in June 2024 and one in April 2024. As is presented in Fig. B.14 and Table A.1, using a mask containing Si III lines, we detect a definite magnetic field $\langle B_z \rangle = 430 \pm 235$ G with FAP = 2×10^{-6} in the primary component. Both components appeared overlapped during the second observation on June 20 2024. We achieved for this observation a marginal detection $\langle B_z \rangle = -373 \pm 38$ G with FAP = 2×10^{-5} using a mask with He I/II and Si III lines. In the third observation acquired on April 16 2025, we detect Zeeman signatures in both components, but a definite field detection using a line mask with He I/II lines, $\langle B_z \rangle = 25 \pm 68$ G with FAP = 9×10^{-6}, corresponds to the more massive component shifted to the blue. For the lower-mass component shifted to the red, we achieve a marginal detection $\langle B_z \rangle = 146 \pm 275$ G with FAP = 2×10^{-4}. More observations are necessary to verify whether both components in this system are magnetic.

4. Discussion

Despite the progress achieved in previous surveys of the magnetism in massive stars, the origin of their magnetic fields remains the least understood topic. The presented study aims to detect magnetic fields and to characterise their strengths in massive binary and multiple systems with components at different stages of interaction. Our sample comprises eight close systems with different contact configurations, one post-RLOF system, one merger, three semi-detached systems, and one detached system. As the longitudinal magnetic field is strongly dependent on the viewing angle between the field orientation and the observer and is modulated as the star rotates, we intended to observe each system at least at two different observing epochs. The number of available spectropolarimetric observations ranged from two observations (e.g. for TU Mus and V356 Sgr) up to eleven observations for μ^{01} Sco. The semi-detached system SV Cen and the triple system HR 6187, suggested to comprise a merger, were observed only once. As is shown in Table A.1, the analysis of 53 high-resolution HARPSpol spectra acquired over the last two years reveals the definite presence of a magnetic field in all studied systems apart from the rather faint system SV Cen, for which only a marginal detection was achieved. The lowest longitudinal magnetic field strength of the order of only a few tens of Gauss was measured for the post-RLOF SB2 system V918 Sco with two supergiant components (Rauw et al. 2001). The measured mean longitudinal magnetic field strengths for all other targets are of the order of a few hundred Gauss to a few kiloGauss.

To understand the implication of the contact configuration and evolutionary state of the studied systems on the magnetic field strengths, we considered for each system the spectral classification of the components, their mass ratio, and the fillout factor. The strongest longitudinal magnetic fields of 4–5 kG were discovered in the massive O-type triple system MY Ser in both components of the contact binary with an orbital period of 3.3216 d, a mass ratio $q = 0.95$, and a fillout factor of 1.99. For the more massive O7.5 III component in this binary, we obtained a definite field detection of about 4 kG at one epoch and a marginal detection $\langle B_z \rangle = 8619 \pm 662$ G at another epoch. Obviously, spectropolarimetric monitoring over the rotation periods of the components is urgently needed to study the structure of such extremely strong magnetic fields in the components of the contact system. As such a strong longitudinal magnetic field has

never been detected in contact binaries in the past, our measurements strongly suggest that interaction between the components in contact systems is of great importance for the generation of magnetic fields. Notably, because the amplitudes of the Zeeman signatures are lower in multiple systems in comparison with the size of these features in single stars (e.g. Hubrig et al. 2023), their magnetic fields can even be stronger. According to the spectral classification of this system, O7.5 III+O9.5 III+O9.5 I, it is already evolved from the main sequence. Importantly, the fillout factor for this system is the largest among all studied systems.

Apart from MY Ser, only two other studied systems have a mass ratio close to 1. These two systems with almost identical component masses are the contact eclipsing system O9.5 V+O9.5 V in the quadruple system V402 Pup with an orbital period of 1.019 d and a fillout factor of 1.31, and the contact eclipsing system B1-1.5 V+B1-1.5 V with an orbital period of 0.762 d and a fillout factor of 1.55 belonging to the system V701 Sco. While the measurement of the magnetic field in the quadruple system is very demanding, the magnetic field measured in the system V701 Sco is rather strong with $\langle B_z \rangle = 678 \pm 150$ G (FAP = 10^{-7}) detected at one epoch and $\langle B_z \rangle = -876 \pm 105$ G (FAP = 4×10^{-4}) measured at another epoch. For this system, we concluded that both B-type components are magnetic.

For a number of systems, in particular systems with B-type components, the detected Zeeman signatures do not extend over the full LSD Stokes I profile. As has already been discussed by Hubrig et al. (2025), this can be explained by the fact that magnetic B-type stars are characterised by a chemical abundance distribution that is non-uniform and non-symmetric with respect to the rotation axis, but shows some symmetry between the topology of the magnetic field and the chemical spot distribution. A rotation modulation of intensities and radial velocities of He and metal lines has also been discovered in magnetic O-type stars (e.g. Grunhut et al. 2012). The authors suggested that the observed line profile variability can be a result of variations in the flattened distribution of magnetospheric plasma around the magnetic star.

While MY Ser appears to be a record holder among the studied systems, kiloGauss-order magnetic fields were also detected in two other systems. We measured $\langle B_z \rangle = 1559 \pm 131$ G with FAP $< 10^{-10}$ in the detached O9.5IV(n)+B0V system V1294 Sco with an orbital period of 5.6 d and a mass ratio of 0.75. A mean longitudinal magnetic field $\langle B_z \rangle = 1327 \pm 128$ G with FAP $< 10^{-10}$ was measured in the triple system V606 Cen hosting a contact B0.5 V+B3 V system with an orbital period of 1.495 d, a mass ratio of 0.55, and a very low fillout factor of 2%.

Admittedly, the number of systems studied is still too low for us to be able to test possible correlations between the occurrence of strong magnetic fields and system characteristics. On the other hand, some characteristics, such as the presence of additional bodies in the system, mass ratios between the components, and probably large fillout factors corresponding to deeper contacts seem to be favourable for the detection of stronger magnetic fields in interacting systems. In any case, the fact that the presence of magnetic fields is detected in all but one of the studied systems strongly suggests that interaction between the system components plays a definite role in the generation of magnetic fields in massive stars.

In contrast, previous surveys of magnetic fields in massive stars reported only a very low occurrence of magnetic fields and usually concentrated on presumably single stars or members of wide binaries. These surveys avoided complex systems with interacting binaries and frequently used inadequate measurement strategies. The best example for a lack of success in the description of the magnetic companion in the interacting system Plaskett's star was demonstrated in the works of Grunhut et al. (2013, 2022). Only a little more than a dozen bona fide contact systems have been reported in the literature (e.g. Abdul-Masih 2025, and references therein). Although our results on magnetic field measurements in interacting binaries present the first assessment of the occurrence rate of magnetic fields in a sample of such systems, additional spectropolarimetric observations are necessary to better understand which evolutionary channels dominate in the magnetic field generation and which end products of such systems hosting magnetic fields are produced.

Knowledge about the presence of magnetic components in contact systems is especially important in view of theoretical modelling that considers them as potential progenitors of gravitational wave sources detectable by facilities such as the Laser Interferometer Gravitational-Wave Observatory (LIGO; Abramovici et al. 1992) and the Virgo Interferometer (Virgo; Abbott et al. 2016). As was already mentioned in Sect. 1, among the well-studied contact systems, almost 70% have at least one confirmed companion and about 25% have more than one additional companion (Abdul-Masih 2025). The author reviewed the current state of the field of massive contact binary observations and suggested that the high multiplicity statistics is not entirely unexpected due to the compactness of the inner orbits and that it is possible that the companion may play a role in the formation of the contact systems. Indeed, multiple systems are important in various astrophysical phenomena, significantly contributing to the genesis of black holes, neutron stars, and progenitors of stellar explosions and mergers. Several studies of the evolutionary pathways of triple systems with non-magnetic components demonstrated their importance for our understanding of the formation of compact object binaries, the production of explosive transients, and gravitational wave sources (e.g. Toonen et al. 2016).

Especially intriguing are studies exploring the role of the third body for producing binary black holes (BBHs) that have the potential to merge within the age of the Universe. According to Vigna-Gómez et al. (2025), for triples in low metallicities and in which the inner binary does not undergo a stellar merger, a BBH may form and the merger of BBHs can be facilitated by a tertiary companion with an orbital period of up to a few thousand days. In favourable orbital configurations, the time-to-coalescence may be as short as the von Zeipel–Lidov–Kozai (ZLK; von Zeipel 1910; Lidov 1962; Kozai 1962) mechanism timescale. Dorozsmai et al. (2024) focussed on the evolution of hierarchical triples in which the stars of the inner binaries are chemically homogeneously evolving and demonstrated that triple systems such as these can experience tertiary mass transfer onto a BBH. The evolution of multiple systems is, however, especially complex and is affected by several bodies dynamics and tidal and mass transfer processes. Obviously, a particularly careful analysis of a representative sample of contact systems is necessary to test theoretical predictions. Our results showing a high occurrence rate of magnetic fields in interacting systems, frequently appearing as members of multiple systems, additionally increase the complexity of evolutionary stellar models of massive systems.

Acknowledgements. We would like to thank the referee Gautier Mathys for his useful comments. Our work is based on observations made with ESO telescopes at the La Silla Paranal Observatory under programmes 087.D-0800(A), 0113.D-0359(B), 0114.D-0183(A), 0115.D-2108(A), and 0115.D-2150(A). One observation was obtained with the Canada-France-Hawaii Telescope, which is operated by the National Research Council of Canada, the Institut National des

Sciences de l'Univers of the Centre National de la Recherche Scientifique of France, and the University of Hawaii.

References

Abbott, B. P., Abbott, R., Abbott, T. D., et al. 2016, Phys. Rev. X, 6, 041015
Abdul-Masih, M. 2025, Contrib. Astron. Observ. Skalnate Pleso, 55, 390
Abdul-Masih, M., Escorza, A., Menon, A., Mahy, L., & Marchant, P. 2022, A&A, 666, A18
Abramovici, A., Althouse, W. E., Drever, R. W. P., et al. 1992, Science, 256, 325
Antokhina, E. A., Srinivasa Rao, M., & Parthasarathy, M. 2011, New A, 16, 177
Appenzeller, I., Fricke, K., Fürtig, W., et al. 1998, The Messenger, 94, 1
Bagnuolo, Jr., W. G., Gies, D. R., Hahula, M. E., Wiemker, R., & Wiggs, M. S. 1994, ApJ, 423, 446
Budding, E., Butland, R., & Blackford, M. 2015, MNRAS, 448, 3784
Burssens, S., Simón-Díaz, S., Bowman, D. M., et al. 2020, A&A, 639, A81
Bychkov, V. D., Bychkova, L. V., & Madej, J. 2016, MNRAS, 455, 2567
Campbell, C. G. 2018, Magnetohydrodynamics in Binary Stars, 456
Davis, P. J., Siess, L., & Deschamps, R. 2014, A&A, 570, A25
De Becker, M. 2018, A&A, 620, A144
De Becker, M., & Raucq, F. 2013, A&A, 558, A28
De Greve, J. P., & Linnell, A. P. 1994, A&A, 291, 786
de Mink, S. E., Pols, O. R., & Hilditch, R. W. 2007, A&A, 467, 1181
Deschamps, R., Siess, L., Davis, P. J., & Jorissen, A. 2013, A&A, 557, A40
Donati, J. F., Semel, M., & Rees, D. E. 1992, A&A, 265, 669
Donati, J. F., Semel, M., Carter, B. D., Rees, D. E., & Collier Cameron, A. 1997, MNRAS, 291, 658
Dorozsmai, A., Toonen, S., Vigna-Gómez, A., de Mink, S. E., & Kummer, F. 2024, MNRAS, 527, 9782
Drechsel, H. 1994, in Astronomische Gesellschaft Abstract Series, 10, 95
Eggen, O. J. 1961, Roy. Greenwich Observ. Bull., 27, 61
Ferrario, L., Pringle, J. E., Tout, C. A., & Wickramasinghe, D. T. 2009, MNRAS, 400, L71
Gagnier, D., & Pejcha, O. 2023, A&A, 674, A121
García-Segura, G., Taam, R. E., & Ricker, P. M. 2021, ApJ, 914, 111
Gratton, R., Squicciarini, V., Nascimbeni, V., et al. 2023, A&A, 678, A93
Grunhut, J. H., Wade, G. A., Sundqvist, J. O., et al. 2012, MNRAS, 426, 2208
Grunhut, J. H., Wade, G. A., Leutenegger, M., et al. 2013, MNRAS, 428, 1686
Grunhut, J. H., Wade, G. A., Folsom, C. P., et al. 2022, MNRAS, 512, 1944
Henneco, J., Schneider, F. R. N., & Laplace, E. 2024, A&A, 682, A169
Hubrig, S., Ilyin, I., Schöller, M., & Lo Curto, G. 2013, Astron. Nachr., 334, 1093
Hubrig, S., Järvinen, S. P., Madej, J., et al. 2018, MNRAS, 477, 3791
Hubrig, S., Järvinen, S. P., Ilyin, I., Schöller, M., & Jayaraman, R. 2023, MNRAS, 521, 6228
Hubrig, S., Schöller, M., Järvinen, S. P., et al. 2024, A&A, 686, L4
Hubrig, S., Järvinen, S. P., Ilyin, I., & Schöller, M. 2025, A&A, 701, A255
Ibanoglu, C., Çakırlı, Ö., & Sipahi, E. 2013, MNRAS, 436, 750
Järvinen, S. P., Hubrig, S., Mathys, G., et al. 2020, MNRAS, 499, 2734
Kippenhahn, R., & Weigert, A. 1967, ZAp, 65, 251
Kozai, Y. 1962, AJ, 67, 591
Leung, K. C., & Schneider, D. P. 1978, ApJ, 222, 924
Li, F. X., Liao, W. P., Qian, S. B., et al. 2022, ApJ, 924, 30
Lidov, M. L. 1962, Planet. Space Sci., 9, 719
Lomax, J. R., Fullard, A. G., Malatesta, M. A., et al. 2017, MNRAS, 464, 1936
Lorenzo, J., Simón-Díaz, S., Negueruela, I., et al. 2017, A&A, 606, A54
Lorenz, R., Mayer, P., & Drechsel, H. 1999, A&A, 345, 531
Mahy, L., Gosset, E., Manfroid, J., et al. 2018, A&A, 616, A75
Maíz-Apellániz, J., Walborn, N. R., Galué, H. Á., & Wei, L. H. 2004, ApJS, 151, 103
Marchant, P., & Bodensteiner, J. 2024, ARA&A, 62, 21
Mochnacki, S. W., & Doughty, N. A. 1972, MNRAS, 156, 51
Offner, S. S. R., Moe, M., Kratter, K. M., et al. 2023, in Astronomical Society of the Pacific Conference Series, 534, Protostars and Planets VII, eds. S. Inutsuka, Y. Aikawa, T. Muto, K. Tomida, & M. Tamura, 275
Ondratschek, P. A., Röpke, F. K., Schneider, F. R. N., et al. 2022, A&A, 660, L8
Pablo, H., Richardson, N. D., & Moffat, A. F. J. 2018, in 3rd BRITE Science Conference, 8, eds. G. A. Wade, D. Baade, J. A. Guzik, & R. Smolec, 101
Penny, L. R., Ouzts, C., & Gies, D. R. 2008, ApJ, 681, 554
Qian, S. B., Liu, L., & Kreiner, J. M. 2006, New A, 12, 117
Qian, S. B., Yuan, J. Z., Liu, L., et al. 2007, MNRAS, 380, 1599
Raucq, F., Rauw, G., Gosset, E., et al. 2016, A&A, 588, A10
Raucq, F., Gosset, E., Rauw, G., et al. 2017, A&A, 601, A133
Rauw, G., Nazé, Y., Carrier, F., et al. 2001, A&A, 368, 212
Rauw, G., Rosu, S., Noels, A., et al. 2016, A&A, 594, A33
Rosu, S., Rauw, G., Nazé, Y., Gosset, E., & Sterken, C. 2022, A&A, 664, A98
Rucinski, S. M., Baade, D., Lu, W. X., & Udalski, A. 1992, AJ, 103, 573
Sana, H., Nazé, Y., O'Donnell, B., Rauw, G., & Gosset, E. 2008, New A, 13, 202
Sana, H., de Mink, S. E., de Koter, A., et al. 2012, Science, 337, 444
Schneider, F. R. N., Podsiadlowski, P., Langer, N., Castro, N., & Fossati, L. 2016, MNRAS, 457, 2355
Schneider, F. R. N., Ohlmann, S. T., Podsiadlowski, P., et al. 2019, Nature, 574, 211
Sen, K., Langer, N., Marchant, P., et al. 2022, A&A, 659, A98
Snik, F., Jeffers, S., Keller, C., et al. 2008, SPIE Conf. Ser., 7014, 70140O
Sota, A., Maíz Apellániz, J., Morrell, N. I., et al. 2014, ApJS, 211, 10
Stickland, D. J., Sahade, J., & Henrichs, H. 1996, The Observatory, 116, 85
Thaller, M. L. 1998, in Astronomical Society of the Pacific Conference Series, 131, Properties of Hot Luminous Stars, ed. I. Howarth, 417
Toonen, S., Hamers, A., & Portegies Zwart, S. 2016, Computat. Astrophys. Cosmol., 3, 6
Tout, C. A., Wickramasinghe, D. T., Liebert, J., Ferrario, L., & Pringle, J. E. 2008, MNRAS, 387, 897
Tüysüz, M., Soydugan, F., Bilir, S., et al. 2014, New A, 28, 44
van Antwerpen, C., & Moon, T. 2010, MNRAS, 401, 2059
van Hamme, W., & Wilson, R. E. 1990, AJ, 100, 1981
van Rensbergen, W., de Greve, J. P., Mennekens, N., Jansen, K., & de Loore, C. 2011, A&A, 528, A16
Vanbeveren, D., De Loore, C., & Van Rensbergen, W. 1998, A&A Rev., 9, 63
Vigna-Gómez, A., Grishin, E., Stegmann, J., et al. 2025, A&A, 699, A272
von Zeipel, H. 1910, Astron. Nachr., 183, 345
Vrancken, J., Abdul-Masih, M., Escorza, A., et al. 2024, A&A, 691, A150
Wellstein, S., Langer, N., & Braun, H. 2001, A&A, 369, 939
Wickramasinghe, D. T., Tout, C. A., & Ferrario, L. 2014, MNRAS, 437, 675
Yang, Y., Yuan, H., & Dai, H. 2019, AJ, 157, 111

Appendix A: Logbook of our observations and magnetic field measurements

In Table A.1, we present the logbook of our observations and the results of the magnetic field measurements for all the systems we studied.

Appendix B: LSD analysis

In Figs. B.1-B.14, we present the results of our LSD analysis, the Stokes I, Stokes V, and diagnostic null N spectra obtained for different line masks. The identified Zeeman signatures are presented in blue colour.

Table A.1. Logbook of observations and results of magnetic field measurements for the studied systems.

Target	Date	MJD	S/N	Line mask	FAP	Det. flag	$\langle B_z \rangle$ [G]	Remark
γ Equ	2024-06-18	60479.41	316	Fe I, La II, Pr III, Nd II	$< 10^{-10}$	DD	−1027±44	
29 CMa	2013-03-03	56354.31	507	He I/II, N III, O II/III, Si III/IV	1×10^{-6}	DD	−26±19	ESPaDOnS
	2024-01-02	60311.04	328	He I, N III	6×10^{-4}	MD	−50±25	
	2024-01-04	60313.04	307	He I/II, C IV, O III	7×10^{-4}	MD	27±7	
	2024-06-17	60478.95	230	He I/II	$< 1 \times 10^{-10}$	DD	−159±113	
	2024-06-18	60479.96	162	He I/II, Si IV	2×10^{-5}	MD	73±27	
	2024-06-19	60480.96	230	He I/II, N III, Si IV	$< 1 \times 10^{-10}$	DD	298±59	
	2025-04-15	60781.07	437	He I/II, N III, O III, Si IV	$< 1 \times 10^{-10}$	DD	56±16	
V402 Pup	2025-04-15	60780.07	148	He I/II	9×10^{-5}	MD		
	2025-04-16	60781.11	177	He I/II, O III	2×10^{-6}	DD	−353±67	
TU Mus	2024-06-18	60479.05	90	He I/II	10^{-5}	DD	482±198	
	2024-06-18	60480.01	128	He I/II	7×10^{-4}	MD		
	2025-04-14	60779.22	205	He I/II C IV	2×10^{-6}	DD		
SV Cen	2024-06-19	60480.09	91	He I, Si III	10^{-3}	MD		
V606 Cen	2024-06-18	60479.15	55	He I,C III, Si III	4×10^{-4}	MD		
	2024-06-19	60481.01	113	He I/II, Si III	2×10^{-6}	DD	−419±168	
	2025-04-14	60777.26	150	He I/II,Al III, Si III	—	ND		
	2025-04-16	60779.29	137	He I/II,Al III, Si III	$< 10^{-10}$	DD	1327±128	
V889 Cen	2024-06-20	60481.08	31	He I/II	10^{-9}	DD		
	2024-06-20	60482.03	24	He I/II, C IV	6×10^{-4}	MD		
	2025-04-14	60779.14	46	He II, C IV	6×10^{-7}	DD		
	2025-04-15	60780.22	33	He I/II, C IV	—	ND		
	2025-04-16	60781.19	49	He I/II, C IV	$< 10^{-10}$	DD		
V918 Sco	2024-06-18	60479.10	289	He I/II, C IV, N III, Si III	6×10^{-6}	DD	45±31	
	2024-06-20	60481.34	245	He I/II, N III, O III, Si IV	9×10^{-8}	DD		
	2025-04-12	60777.38	612	He I/II, C IV, N III, O III	3×10^{-4}	MD	−11±6	
	2025-04-15	60780.27	589	He I/II, C IV, O III, Si III	$< 10^{-10}$	DD		
HR 6187	2024-06-17	60478.99	227	He I/II, C IV, N III	6×10^{-6}	DD	−369±58	
μ^{01} Sco	2024-06-18	60479.35	322	He I, Si III	10^{-5}	DD	242±55	
	2024-06-19	60480.14	323	He I, Si III	2×10^{-4}	MD	−187±29	
	2024-06-20	60481.32	278	He I, Si III	4×10^{-6}	DD		
	2024-06-20	60481.99	275	He I	2×10^{-9}	DD		
	2025-04-13	60778.41	612	He I, Si II/III	10^{-7}	DD		
	2025-04-13	60778.41	583	He I, Si III	—	ND		
	2025-04-13	60778.42	645	He I, Si II/III	10^{-4}	MD		
	2025-04-13	60778.42	641	He I, Si II/III	—	ND		
	2025-04-13	60778.43	585	He I, Si II/III	$< 10^{-10}$	DD		
	2025-04-14	60779.40	653	He I, Si III	2×10^{-5}	MD		
	2025-04-14	60779.41	637	He I, Si III	2×10^{-4}	MD		

Notes. The first column lists the target name, followed by the date of the observation, the MJD values at the middle of the exposure, the signal to noise ratio (S/N) measured in the Stokes I spectra in the spectral region around 5000 Å, the line mask used, the FAP values, the detection flag – where DD means definite detection, MD marginal detection, and ND no detection, – the measured LSD mean longitudinal magnetic field strength, and a remark on the Stokes V feature where the field was diagnosed (if applicable). $\langle B_z \rangle$-values may not be included in all cases due to the complexity of the composite spectra at some observing epochs.

Table A.1. Continued.

Target	Date	MJD	S/N	Line mask	FAP	Det. flag	$\langle B_z \rangle$ [G]	Remark
V1294 Sco	2024-06-20	60481.30	106	He I/II, O III	$< 1 \times 10^{-10}$	DD		
	2025-04-15	60780.39	282	He I/II, C IV, Si III	$< 10^{-10}$	DD	1559±131	
	2025-04-16	60781.25	286	He I/II, O III	2×10^{-7}	DD		
V701 Sco	2024-06-19	60480.18	144	He I, Si III	10^{-7}	DD	678±150	
	2025-04-12	60777.33	240	He I, Si III	4×10^{-4}	MD	−876±105	
	2025-04-14	60779.36	204	He I, Si III	$< 10^{-10}$	DD		
	2025-04-15	60780.33	228	He I, Si III	$< 10^{-10}$	DD		
MY Ser	2024-06-18	60479.31	200	He I/II, C III, N III, O III, Si IV	10^{-7}	DD	−46±31	
	2024-06-19	60480.30	232	He I, C III/IV, O III	3×10^{-8}	DD	4008±402	
	2024-06-20	60481.16	225	He I/II, C III, O III	$< 10^{-10}$	DD		
	2025-04-16	60781.50	363	He I/II, C III	2×10^{-8}	DD	−4875±394	right
				He I/II,N III, O III	4×10^{-5}	MD	8619±662	left
V356 Sgr	2024-06-18	60479.38	190	He I, Si II/III, Fe II	1.5×10^{-7}	DD	856±240	
	2024-06-20	60481.39	223	Mg II, Fe II	7×10^{-6}	DD	−718±245	
V337 Aql	2024-06-18	60479.23	140	Si III	2×10^{-6}	DD	430±235	
	2024-06-20	60481.24	125	He I/II, Si III	2×10^{-5}	MD	−373±38	
	2025-04-16	60781.37	266	He I/II	3×10^{-4}	MD	146±275	right
				He I/II	9×10^{-6}	DD	25±68	left

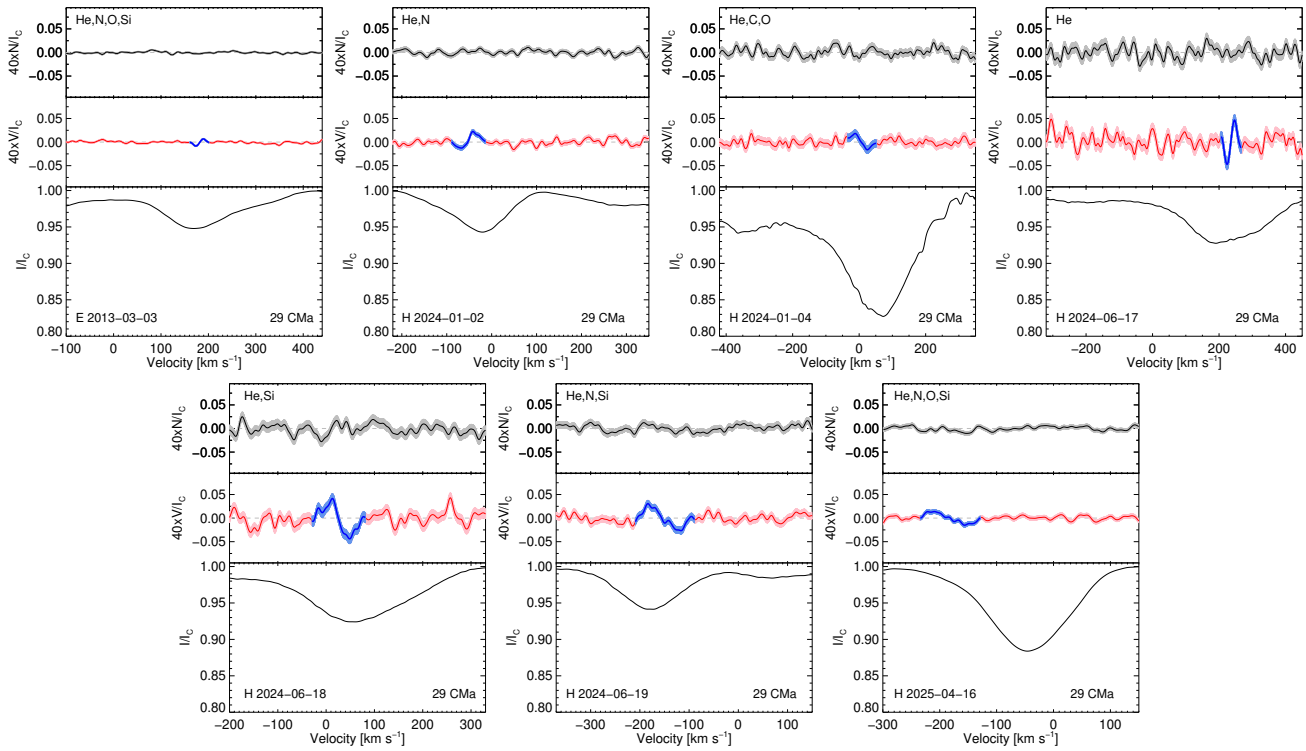

Fig. B.1. Results of our LSD analysis of 29 CMa. Stokes I, Stokes V, and diagnostic null N spectra obtained for different line masks using one archival ESPaDOnS observation and six HARPSpol observations are shown. The identified Zeeman signatures are presented in blue colour.

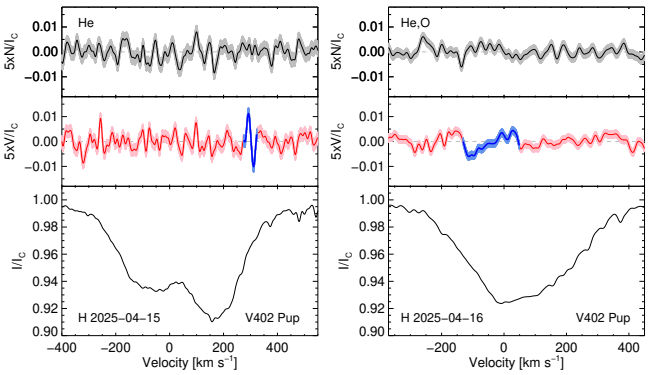

Fig. B.2. As Figure B.1, but for V402 Pup.

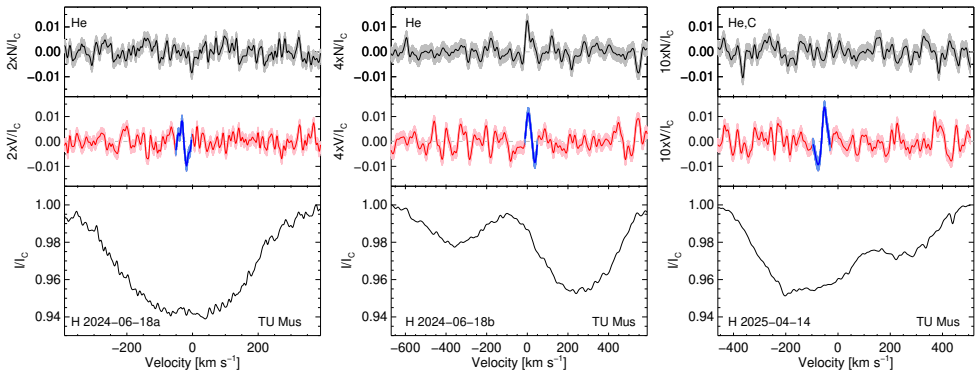

Fig. B.3. As Figure B.1, but for TU Mus.

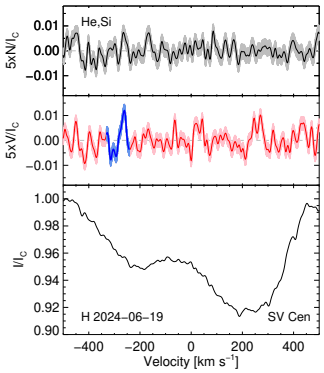

Fig. B.4. As Figure B.1, but for SV Cen.

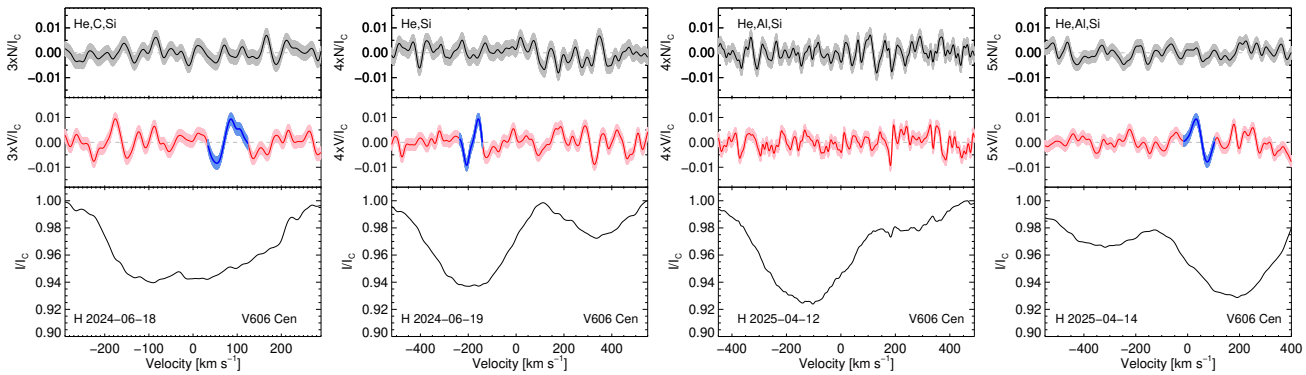

Fig. B.5. As Figure B.1, but for V606 Cen.

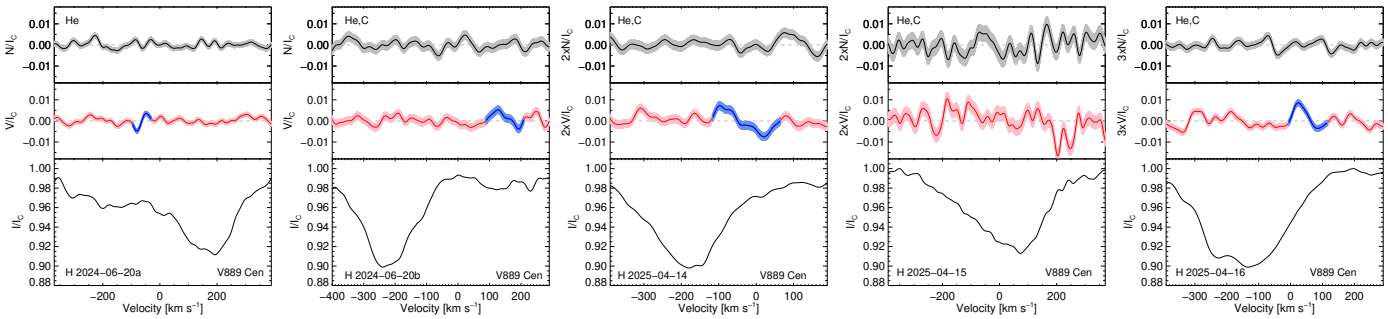

Fig. B.6. As Figure B.1, but for V889 Cen.

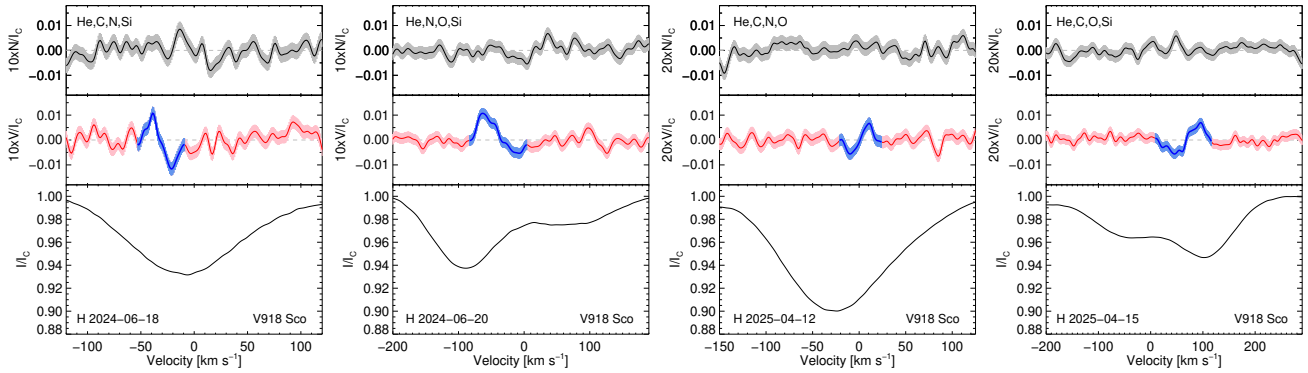

Fig. B.7. As Figure B.1, but for V918 Sco.

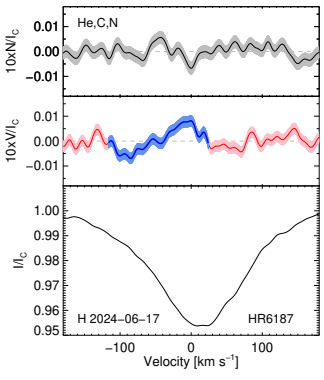

Fig. B.8. As Figure B.1, but for HR 6187.

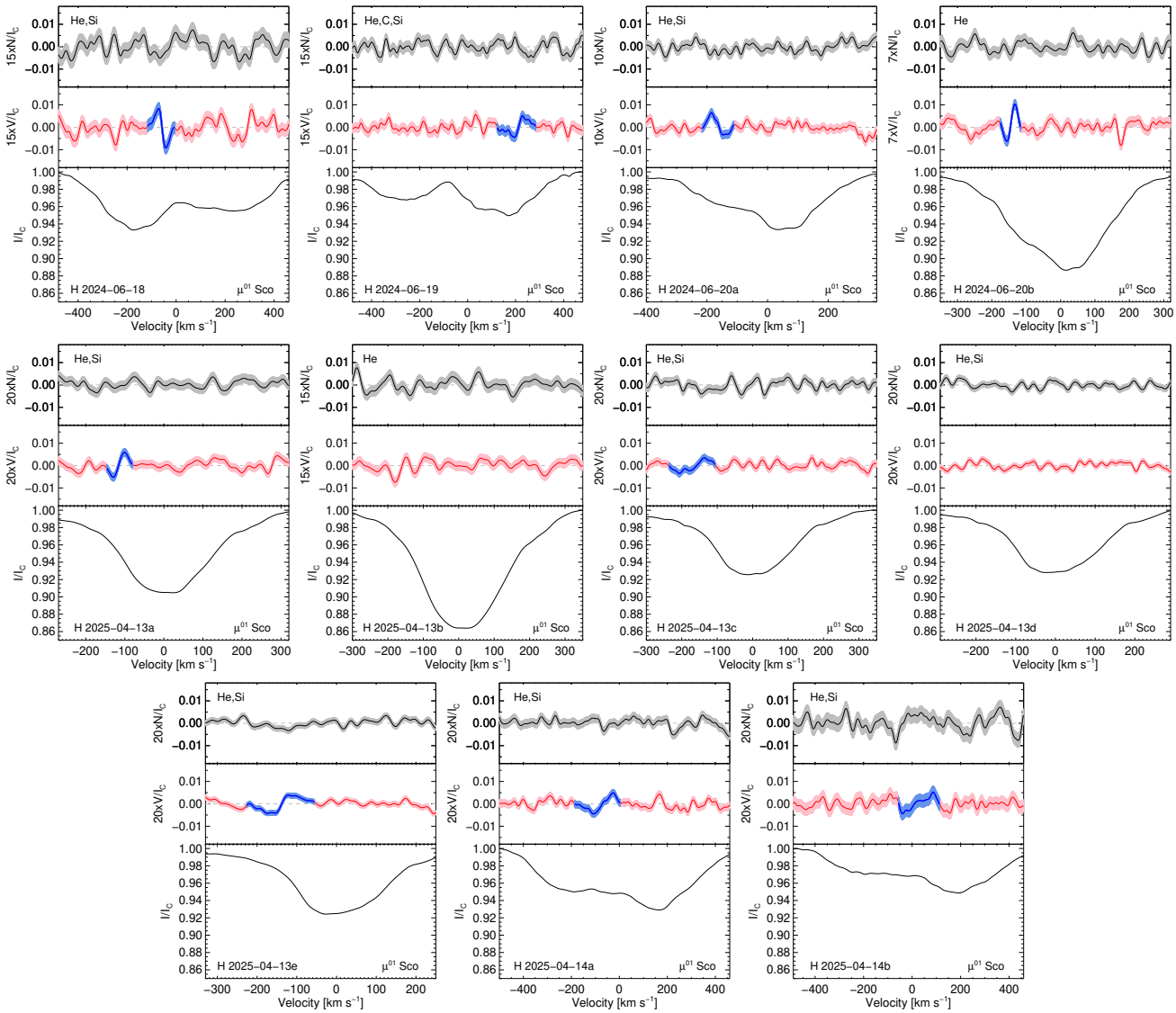

Fig. B.9. As Figure B.1, but for μ^{01} Sco.

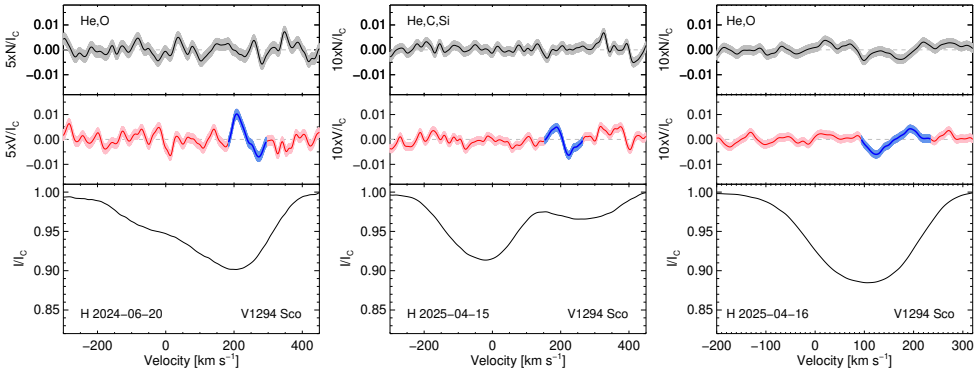

Fig. B.10. As Figure B.1, but for V1294 Sco.

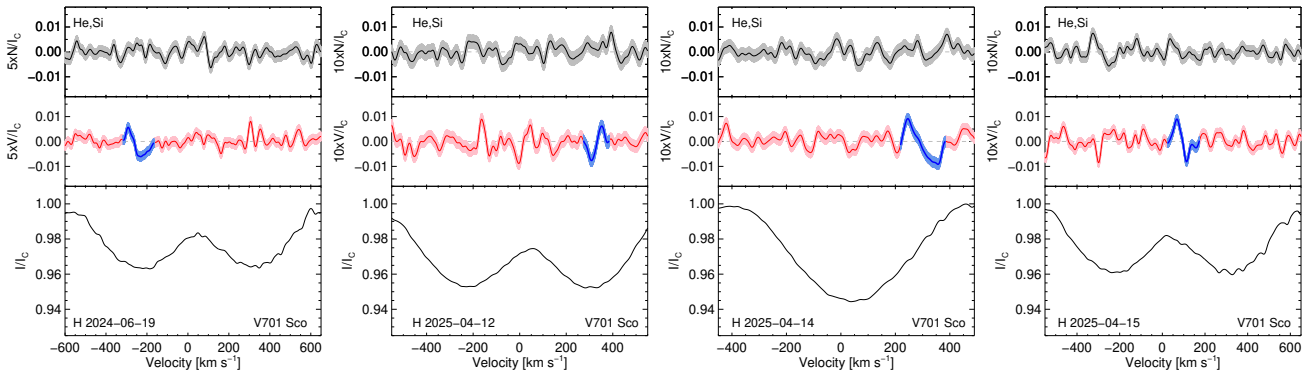

Fig. B.11. As Figure B.1, but for V701 Sco.

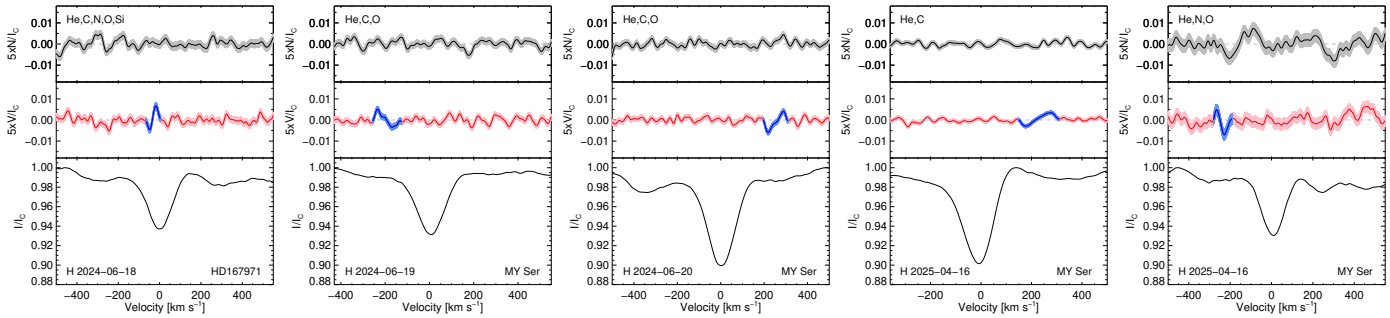

Fig. B.12. As Figure B.1, but for MY Ser.

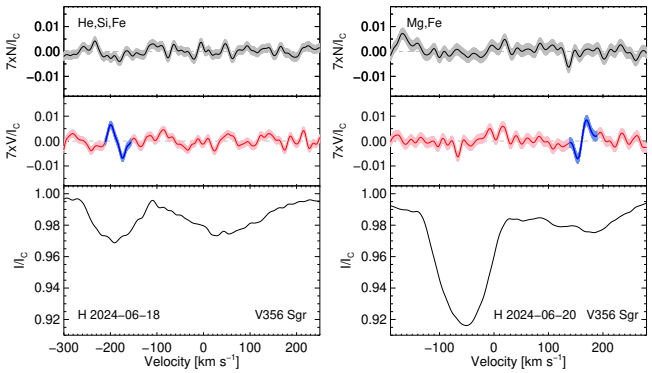

Fig. B.13. As Figure B.1, but for V356 Sgr.

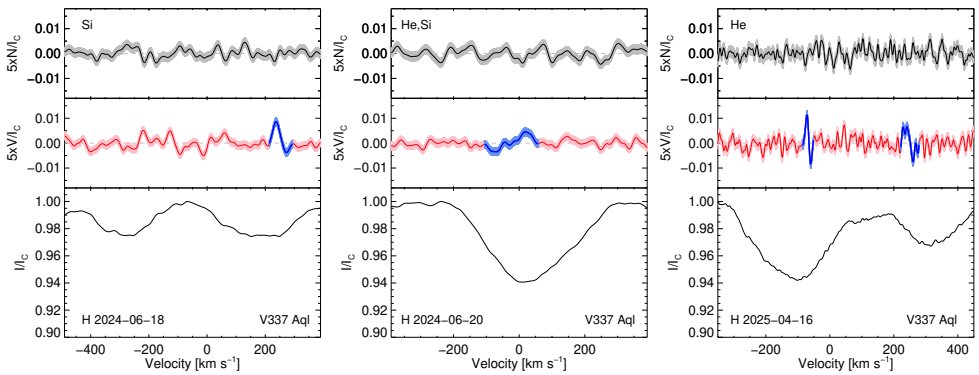

Fig. B.14. As Figure B.1, but for V337 Aql.